

# Thermal excitation of multi-photon dressed states in circuit quantum electrodynamics

J M Fink<sup>1</sup>, M Baur<sup>1</sup>, R Bianchetti<sup>1</sup>, S Filipp<sup>1</sup>, M Göppl<sup>1</sup>, P J Leek<sup>1</sup>, L Steffen<sup>1</sup>, A Blais<sup>2</sup> and A Wallraff<sup>1</sup>

<sup>1</sup> Department of Physics, ETH Zurich, CH-8093 Zurich, Switzerland

<sup>2</sup> Département de Physique, Université de Sherbrooke, Québec J1K 2R1, Canada

E-mail: [jfink@phys.ethz.ch](mailto:jfink@phys.ethz.ch) and [andreas.wallraff@phys.ethz.ch](mailto:andreas.wallraff@phys.ethz.ch)

Received 16 October 2009

Accepted for publication 23 October 2009

Published 14 December 2009

Online at [stacks.iop.org/PhysScr/T137/014013](http://stacks.iop.org/PhysScr/T137/014013)

## Abstract

The exceptionally strong coupling realizable between superconducting qubits and photons stored in an on-chip microwave resonator allows for the detailed study of matter–light interactions in the realm of circuit quantum electrodynamics (QED). Here we investigate the resonant interaction between a single transmon-type multilevel artificial atom and weak thermal and coherent fields. We explore up to three photon dressed states of the coupled system in a linear response heterodyne transmission measurement. The results are in good quantitative agreement with a generalized Jaynes–Cummings model. Our data indicate that the role of thermal fields in resonant cavity QED can be studied in detail using superconducting circuits.

PACS numbers: 42.50.Ct, 42.50.Pq, 03.67.Lx, 85.35.Gv

(Some figures in this article are in colour only in the electronic version.)

## 1. Introduction

In cavity quantum electrodynamics (QED) [1–4] the fundamental interaction of matter and light is studied in a well-controlled environment. On the level of individual quanta this interaction is governed by the Jaynes–Cummings [5] Hamiltonian. In early experiments the quantization of the electromagnetic field was observed in cavity QED with Rydberg atoms by measurements of collapse and revival [6]. Similarly, the  $\sqrt{n}$  scaling of the atom/photon coupling strength with the number of photons  $n$  has been observed in the time domain by measuring  $n$  photon Rabi oscillations using coherent states [7] and Fock states [8, 9]. In the frequency domain the  $\sqrt{n}$  scaling can be extracted from spectroscopic cavity transmission measurements. Initial attempts employing pump and probe spectroscopy with alkali atoms [10] were inconclusive. In a recent experiment however, the two-photon vacuum Rabi resonance was resolved using high-power nonlinear spectroscopy [11]. At the same time, we observed the quantum nonlinearity by measuring the spectrum

of two photons and one artificial atom in circuit QED [12]. In these measurements the originally proposed pump and probe spectroscopy scheme [10] was used. Similarly, the  $n$  photon Rabi mode splitting was studied using multi-photon transitions up to  $n = 5$  [13]. In the dispersive regime the photon number splitting of spectroscopic lines [14] provides similar evidence for the quantization of microwave radiation in circuit QED. Further experimental progress in the time domain has enabled the preparation and detection of coherent states [15], photon number states [16] and arbitrary superpositions of photon number states [17] in circuits. Using Rydberg atoms, quantum jumps of light have been observed [18, 19] and Wigner functions of Fock states have been reconstructed [20]. These experiments demonstrate the quantum nature of light by measuring the nonlinear  $\sqrt{n}$  scaling of the dipole coupling strength with the discrete number of photons  $n$  in the Jaynes–Cummings [21] model.

In this paper we extend our earlier spectroscopic study of the  $\sqrt{n}$  scaling [12] in the circuit QED architecture [22, 23]. We present a measurement of the photon/atom energy

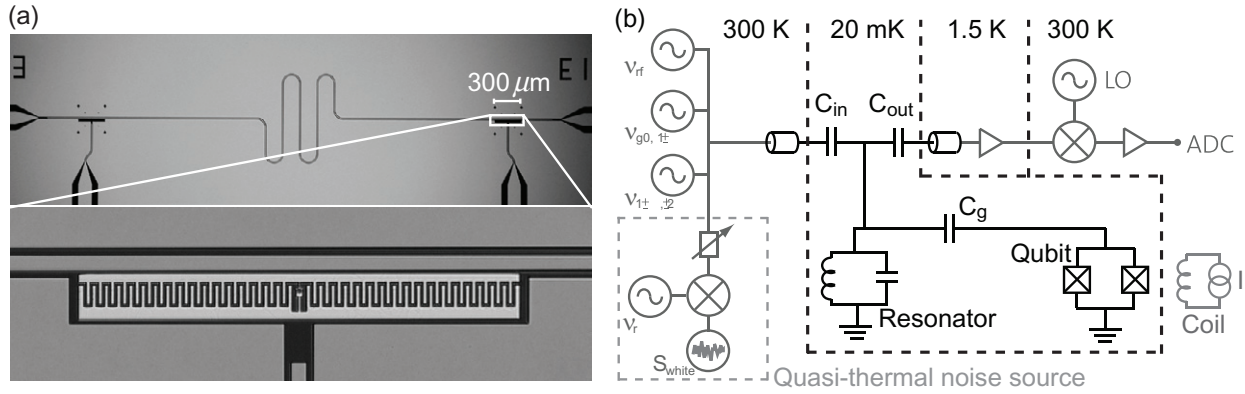


**Figure 1.** Sample and experimental setup. (a) Optical images of the superconducting coplanar waveguide resonator (top) with the transmon-type superconducting qubit embedded at the position indicated. The qubit of dimensions  $300 \times 30 \mu\text{m}^2$  is shown on the bottom. (b) Simplified circuit diagram of the experimental setup. The qubit is capacitively coupled to the resonator through  $C_g$  and flux tuned with a current-biased ( $I$ ) external miniature superconducting coil. The resonator, represented by a parallel LC circuit, is coupled to input and output transmission lines via the capacitors  $C_{\text{in}}$  and  $C_{\text{out}}$ . A quasi-thermal field can be generated by modulating a microwave carrier tone  $\nu_r$  with a large bandwidth pseudo-random noise spectrum  $S_{\text{white}}$ . The noise signal is filtered, attenuated and added to pump ( $\nu_{g0,1\pm}, \nu_{l\pm,2\pm}$ ) and probe ( $\nu_{\text{rf}}$ ) tones. The resulting microwave fields are further attenuated and applied to the resonator input. After amplification with an ultra low noise amplifier, the transmitted probe signal  $\nu_{\text{rf}}$  is downconverted with a local oscillator (LO) and digitized with an analogue to digital converter (ADC).

spectrum up to  $n = 3$  excitations using both thermal and coherent fields. A solid state qubit with a large effective dipole moment plays the role of the atom. It is coupled to weak microwave radiation fields in a coplanar waveguide resonator, which provides a very large electric field strength per photon. The coupling strength of a few hundred MHz [24], much larger than in implementations with natural atoms, can freely be chosen over a wide range of values and remains fixed in time. The qubit level spectrum is *in situ* tunable by applying flux to the circuit and the internal degrees of freedom can be prepared and manipulated with microwave fields.

Similar solid state circuit implementations of cavity QED have enabled a remarkable number of novel quantum optics [12–14, 16, 17, 23, 25–30] and quantum computation [31–33] experiments.

## 2. Sample and experimental setup

For the experiments presented here we use a transmon-type qubit [34, 35], which is a charge-insensitive superconducting qubit design derived from the Cooper pair box [36], as the artificial atom. Its transition frequency is given by  $\omega_{g,e}/2\pi \simeq \sqrt{8E_C E_J(\Phi)} - E_C$  with the single electron charging energy  $E_C/h \approx 0.232$  GHz, the flux-controlled Josephson energy  $E_J(\Phi) = E_{J,\text{max}} |\cos(\pi\Phi/\Phi_0)|$  and  $E_{J,\text{max}}/h \approx 35.1$  GHz, as determined by spectroscopic measurements. The two characteristic energies  $E_J$  and  $E_C$  define the full level spectrum of the qubit where the eigenenergy of level  $l$  is approximately given as  $E_l \simeq -E_J + \sqrt{8E_C E_J}(l+1/2) - E_C/12(6l^2 + 6l + 3)$  [34]. The cavity is realized as a coplanar resonator with bare resonance frequency  $\nu_r \approx 6.44$  GHz and photon decay rate  $\kappa/2\pi \approx 1.6$  MHz. Details of the resonator design and fabrication can be found in [37]. Optical microscope images of the sample are shown in figure 1(a). A simplified electrical circuit diagram of the setup is shown in figure 1(b).

## 3. Generalized Jaynes–Cummings model

The transmon qubit is a superconducting circuit with a nonlinear energy level spectrum. In many experiments the nonlinearity, which can be adjusted by circuit design and fabrication, is sufficient to correctly model it as a two-level system. For the experimental results presented in this work it is, however, essential to treat the qubit as a multilevel system taking into account the coupling of all relevant transmon levels to the cavity photons. The physics of this multilevel artificial atom strongly coupled to a single mode of the electromagnetic field is described by a generalized Jaynes–Cummings model with the Hamiltonian

$$\hat{\mathcal{H}} = \hbar\omega_r \hat{a}^\dagger \hat{a} + \sum_{l=e,f,h,\dots} \left( \hbar\omega_l \hat{\sigma}_{l,l} + \hbar g_{l-1,l} (\hat{\sigma}_{l-1,l}^\dagger \hat{a} + \hat{a}^\dagger \hat{\sigma}_{l-1,l}) \right). \quad (1)$$

Here,  $\hbar\omega_l$  is the energy of the  $l$ th excited state  $|l\rangle$  of the multilevel artificial atom,  $\omega_r$  is the frequency of the resonator field and  $g_{l-1,l}$  is the coupling strength of the transition  $l-1 \rightarrow l$  and one photon.  $\hat{a}^\dagger$  and  $\hat{a}$  are the raising and lowering operators acting on the field with photon number  $n$  and  $\hat{\sigma}_{i,j} = |i\rangle\langle j|$  are the corresponding operators acting on the qubit states. In figure 2, a sketch of the energy level diagram of the resonantly coupled qubit–resonator system ( $\nu_r = \nu_{g,e}$ ) is shown for up to three photons  $n = 0, 1, 2, 3$  and the first four transmon levels  $l = g, e, f$  and  $h$ .

Considering the first two levels of the artificial atom at zero detuning ( $\Delta \equiv \nu_r - \nu_{g,e} = 0$ ), the eigenstates of the coupled system are the symmetric ( $|g, n\rangle + |e, n-1\rangle$ )/ $\sqrt{2} \equiv |n+\rangle$  and antisymmetric ( $|g, n\rangle - |e, n-1\rangle$ )/ $\sqrt{2} \equiv |n-\rangle$  qubit–photon superposition states, see figure 2. For  $n = 1$ , the coupled one-photon one-atom eigenstates are split due to the dipole interaction [38, 39]. These states have been observed in hallmark experiments demonstrating the strong coupling of a single atom and a single photon both spectroscopically as a vacuum Rabi mode splitting with on average a single atom [40] and also without averaging using alkali atoms [41],

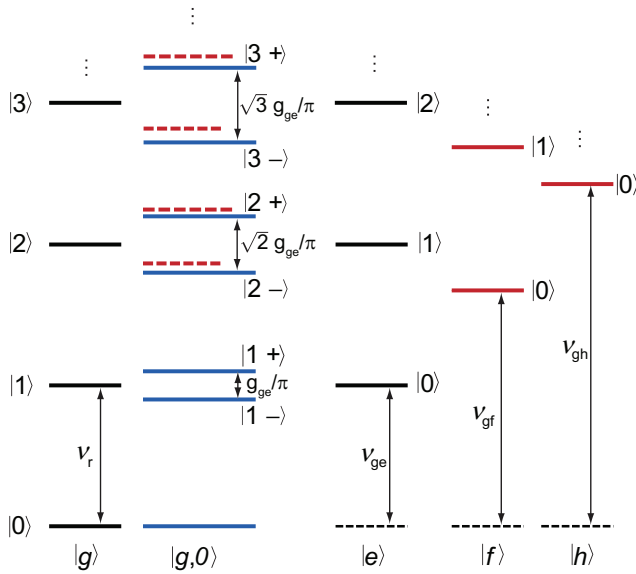


**Figure 2.** Sketch of the energy level diagram of a resonant ( $\nu_r = \nu_{g,e}$ ) cavity QED system. The uncoupled qubit states  $|g\rangle$ ,  $|e\rangle$ ,  $|f\rangle$  and  $|h\rangle$  (from left to right) and the photon states  $|0\rangle$ ,  $|1\rangle$ ,  $|2\rangle$ ,  $|3\rangle$ , ... (from bottom to top) are shown with black and red solid lines. The dipole-coupled dressed states are shown in blue and the shifts due to the  $|f, 0\rangle$  and  $|h, 0\rangle$  levels are indicated by red dashed lines.

in superconducting circuits [23] and semiconducting quantum dot systems [42, 43], or in time-resolved measurements as vacuum Rabi oscillations at frequency  $2g_{g,e}$  with Rydberg atoms [7, 8] and superconducting circuits [15, 16]. At least in principle however, the observation of the first doublet  $|1\pm\rangle$  alone could also be explained as normal mode splitting in a classical linear dispersion theory [44]. The Jaynes–Cummings model however predicts a characteristic nonlinear scaling of this frequency as  $\sqrt{n}2g_{g,e}$  with the number of excitations  $n$  in the system. In the general multilevel case, the higher energy atomic levels renormalize the dipole-coupled dressed state energies. This causes frequency shifts in the excitation spectrum as indicated in figure 2 and the simple  $\sqrt{n}$  scaling is slightly modified.

#### 4. Vacuum Rabi mode splitting in the presence of a thermal field

In this section we investigate vacuum Rabi resonances both in the presence of a weak thermal background field and in the presence of externally applied quasi-thermal fields. To our knowledge this is the first experiment where thermally excited multiphoton dressed states are studied systematically in a cavity QED system.

Experimentally, the coupled circuit QED system is prepared in its ground state  $|g, 0\rangle$  by cooling it to temperatures below  $< 20$  mK in a dilution refrigerator. Measuring the cavity transmission spectrum  $T$  in the anti-crossing region of the qubit transition frequency  $\nu_{g,e}$  and the cavity frequency  $\nu_r$  yields transmission maxima at frequencies corresponding to transitions from  $|g, 0\rangle$  to the first doublet  $|1\pm\rangle$  of the Jaynes–Cummings ladder, see figure 3(a). On resonance, see figure 3(b), we extract the coupling strength of  $g_{g,e}/2\pi = 133$  MHz. This is a clear indication that the strong coupling

limit  $g_{g,e} \gg \kappa, \gamma$ , with photon decay and qubit decoherence rates  $\kappa/2\pi, \gamma/2\pi \sim 1$  MHz, is realized. The solid lines in figure 3(a) (and figure 4(a)) are numerically calculated dressed state frequencies, see figure 3(c), with the qubit and resonator parameters as stated above. For the calculation, the qubit Hamiltonian is diagonalized exactly in the charge basis. The qubit states  $|g\rangle$  and  $|e\rangle$  and the flux-dependent coupling constant  $g_{g,e}$  are then incorporated in the Jaynes–Cummings Hamiltonian equation (1). Its numerical diagonalization yields the dressed states of the coupled system without any fit parameters.

In addition to the expected spectral lines corresponding to the transition from the ground state  $|g, 0\rangle$  to the first doublet states  $|1\pm\rangle$ , we observe three lines with very low intensities, see figures 3(a) and (b). These additional transitions are visible because the system is excited by a small thermal background field with a cavity photon number distribution given by the Bose–Einstein distribution. This thermal field is a consequence of incomplete thermalization of the room temperature black-body radiation at the input and output ports of the resonator. A quantitative analysis taking into account the two-photon states  $|2\pm\rangle$  and the presence of the higher energy qubit levels  $f$  and  $h$  in equation (1) yields the transition frequencies indicated by yellow and red solid lines in figure 3. For this analysis the coupling constants  $g_{e,f} = 184$  MHz and  $g_{f,h} = 221$  MHz of higher energy qubit levels to the cavity mode, obtained from exact diagonalization of the qubit Hamiltonian, have been included. We thus identify two of the additional spectral lines as transitions between the first  $|1\pm\rangle$  and second  $|2\pm\rangle$  doublet states of the resonant Jaynes–Cummings ladder, see figure 3(c). The lowest frequency additional spectral line corresponds to a transition from the antisymmetric doublet state with one photon  $|1-\rangle$  to the qubit  $f$  level without a photon  $|f, 0\rangle$ . The details of the thermally excited transmission spectrum can be used as a sensitive probe for the cavity field temperature. Analyzing the amplitudes of the Rabi splitting spectrum with a quantitative master equation model [13] leads to an estimated photon temperature of  $T_r \simeq 0.2$  K, which corresponds to a relatively high mean thermal occupation number of  $\bar{n}_{th} \simeq 0.3$  photons for the data presented in figure 3(a). Careful filtering and thermalization at the input and output ports results in a typical cavity photon temperature of  $< 90$  and  $< 54$  mK ( $\bar{n}_{th} < 0.03$  and  $\bar{n}_{th} < 0.003$ ) as reported in [27] and [13].

In order to access the three-photon doublet states  $|3\pm\rangle$  of the coupled multiphoton multilevel-atom system, we use externally applied broadband quasi-thermal fields. In this new approach the dressed eigenstates are populated according to a thermal distribution depending on the chosen thermal field temperature. This allows us to investigate the flux dependence of all resolvable spectral lines for a given effective resonator mode temperature  $T_r$  in a single experimental run. The spectrum of a one-dimensional black body such as the considered cavity is given as  $S_{ID}(\nu) = h\nu/[\exp(h\nu/k_B T) - 1]$ . At a temperature of  $T_r > h\nu_r/k_B \simeq 300$  mK, this energy spectrum is flat with a deviation of  $< 5\%$  within a 500 MHz band centered at the cavity frequency  $\nu_r \simeq 6.44$  GHz. It is therefore a very good approximation to make use of a white noise spectrum in the narrow frequency band of the experimentally investigated transition frequencies centered at

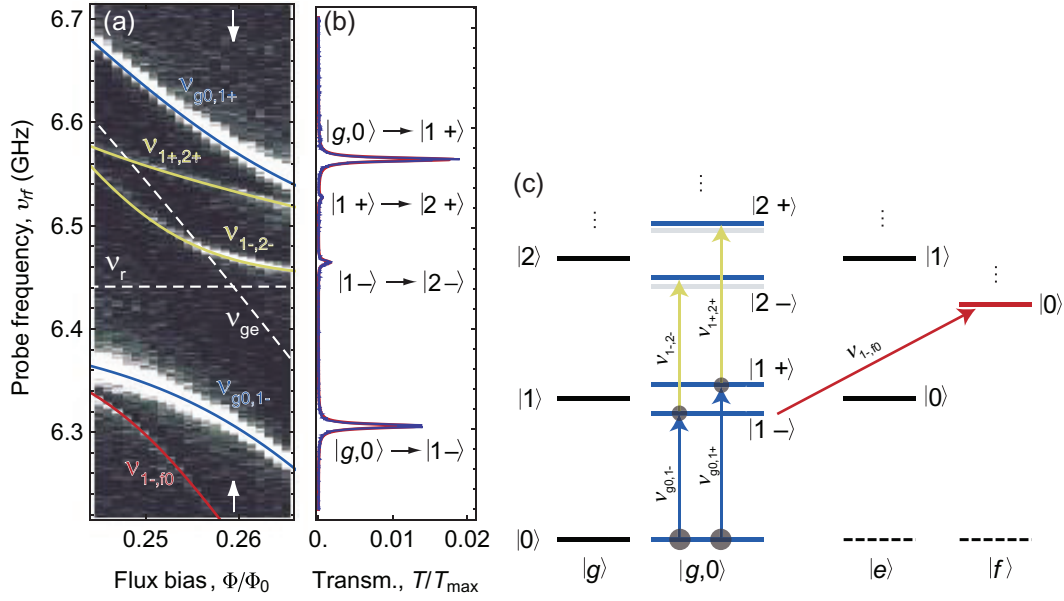


**Figure 3.** Vacuum Rabi mode splitting with a weak coherent probe tone. (a) Measured resonator transmission spectra versus external flux  $\Phi$  close to degeneracy. Black indicates low and white high transmission  $T$ . The solid lines show dressed state energies as obtained numerically and the dashed lines indicate the bare resonator frequency  $\nu_r$  and the qubit transition frequency  $\nu_{g,e}$ . (b) Resonator transmission  $T$  at degeneracy as indicated with arrows in panel (a), with a line fit to four Lorentzians in red. (c) Corresponding energy level spectrum (similar to figure 2) with observed transitions indicated by arrows and small thermal population indicated with gray circles.

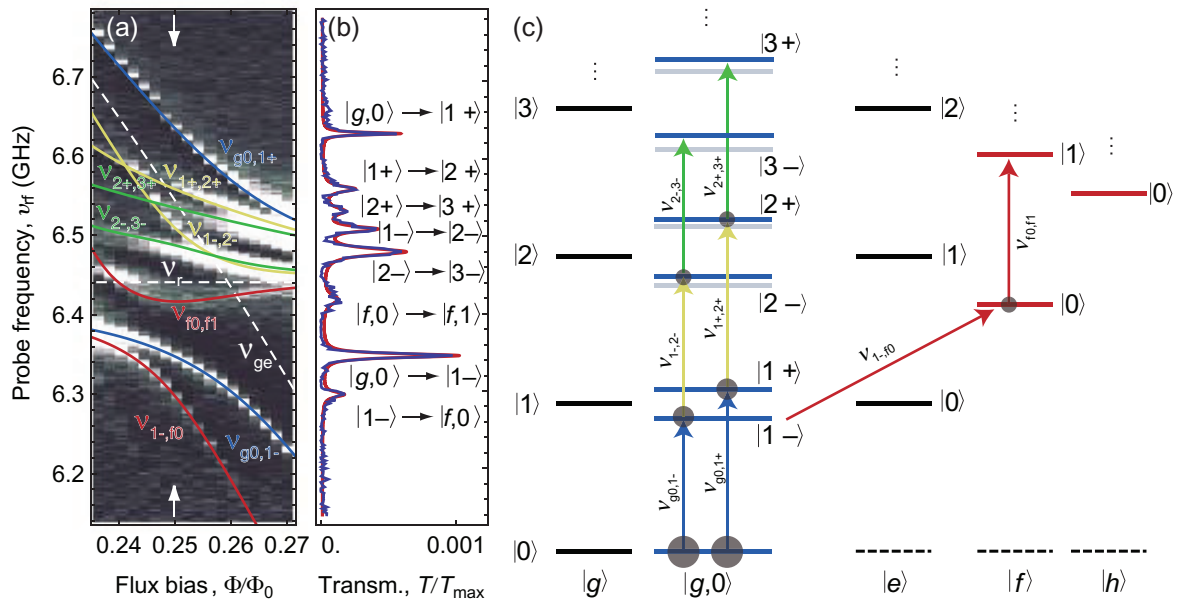


**Figure 4.** Vacuum Rabi mode splitting in the presence of a thermal field. (a) Cavity transmission  $T$  as in figure 3 with an additional quasi-thermal field of temperature  $T_r \sim 0.4$  K applied to the resonator input populating the  $|1\pm\rangle, |2\pm\rangle$  and  $|f, 0\rangle$  states. (b) Transmission spectrum at  $\Phi/\Phi_0 = 0.25$ , indicated by arrows in (a). (c) Corresponding energy level spectrum (similar to figure 2) with observed transitions indicated by arrows and induced thermal population indicated with gray circles.

$\nu_r$ , in order to generate a quasi-thermal field of temperature  $T_r > 300$  mK and populate the considered cavity mode with thermal photons.

In order to generate such a spectrum, a carrier microwave tone at frequency  $\nu_r$  is modulated with a low-frequency large bandwidth quasi-random noise spectrum  $S_{white}$  using a mixer, see figure 1(b). This approximately yields a microwave frequency white noise spectrum with a bandwidth of 500 MHz centered symmetrically around the cavity frequency  $\nu_r$ . Using tunable attenuators, we can adjust the noise power spectral

density over a wide range of values. For this experiment we adjust it such that the thermal population of the cavity mode is on the order of  $\bar{n}_{th} \sim 0.9$  corresponding to a temperature of  $T_r \sim 0.4$  K. This noise spectrum constitutes a sufficient approximation of a black body thermal noise source for the considered 1D cavity mode, temperature and frequency. At the same time, the chosen mean thermal population  $\bar{n}_{th} \sim 0.9$  allows one to observe all allowed transitions between the ground state  $|g\rangle$  and the three-photon doublet states  $|3\pm\rangle$ .

In the presence of the thermal field, we probe the cavity transmission spectrum as a function of flux in the anticrossing region, see figure 4(a), with a weak coherent probe tone  $\nu_{rf}$  in the linear response limit. In this limit the weak probe tone is only a small perturbation to the field and no multi-photon transitions are induced. In this measurement we resolve all allowed transitions between the thermally occupied dipole coupled states in the generalized Jaynes–Cummings ladder. The solid lines are again the calculated dressed state transition energies, which agree well with the observed spectral lines. In figure 4(b), a cavity transmission measurement at flux  $\Phi/\Phi_0 = 0.25$  is shown. We identify eight allowed transitions, compare with figure 4(c). It follows that the states  $|1\pm\rangle$ ,  $|2\pm\rangle$  and also  $|f, 0\rangle$  are thermally populated.

In the two-level-atom approximation, transitions between symmetric and antisymmetric doublet states are forbidden at degeneracy. In the generalized Jaynes–Cummings model, the dressed state transition matrix elements are renormalized due to higher qubit levels. Numerical diagonalization, however, shows that the matrix elements squared, which are related to the amplitude of the expected spectral lines, are 140 (6) times smaller for the symmetry changing transitions  $|1-\rangle \rightarrow |2+\rangle$  ( $|1+\rangle \rightarrow |2-\rangle$ ) than for the observed symmetry preserving transitions  $|1-\rangle \rightarrow |2-\rangle$  ( $|1+\rangle \rightarrow |2+\rangle$ ) at degeneracy. Similarly, for the transitions  $|2-\rangle \rightarrow |3+\rangle$  ( $|2+\rangle \rightarrow |3-\rangle$ ), the matrix elements squared are 235 (16) times smaller than the measured transitions  $|2-\rangle \rightarrow |3-\rangle$  ( $|2+\rangle \rightarrow |3+\rangle$ ) at degeneracy. Therefore transitions between symmetric and antisymmetric doublet states are not resolved in our experiment. Symmetry changing transitions populating the antisymmetric states  $|2-\rangle$  and  $|3-\rangle$  have larger matrix elements than symmetry changing transitions populating the symmetric states  $|2+\rangle$  and  $|3+\rangle$  because the former are closer in frequency to the qubit levels  $|f, 0\rangle$  and  $|h, 0\rangle$ . Similarly, the matrix element for the transition  $|1-\rangle \rightarrow |f, 0\rangle$  is 34 times larger than for the transition  $|1+\rangle \rightarrow |f, 0\rangle$  at degeneracy. The latter is therefore also not observed in the experimental data. In addition to the transition  $|1-\rangle \rightarrow |f, 0\rangle$ , also seen in the data presented in figure 3, we observe a transmission line that corresponds to the transition  $|f, 0\rangle \rightarrow |f, 1\rangle$ , see figure 4(b). A numerical calculation shows that the matrix element is five times larger at degeneracy than  $|2-\rangle \rightarrow |f, 1\rangle$  and seven times larger than  $|f, 0\rangle \rightarrow |h, 0\rangle$ , which in principle could also have been observed. All transitions observed in the experimental data are in qualitative agreement with the calculated matrix elements stated above.

In figure 5 the complete measured level spectrum of the bound photon/atom system up to the third excitation is shown. To calculate the absolute energies of the levels (blue dots), we extract the transition frequencies from data presented in figure 4 with Lorentzian line fits and add them accordingly. For the first doublet states  $|1\pm\rangle$ , we find excellent agreement with both a simple two-level atom Jaynes–Cummings model (dotted red lines) and the generalized multilevel Jaynes–Cummings model (solid red lines). In the case of the second  $|2\pm\rangle$  and third doublet states  $|3\pm\rangle$ , we find considerable frequency shifts with regard to the two-level model (compare the dotted and solid red lines) but excellent agreement with the generalized model taking into account the additional qubit levels. Furthermore, it can be seen

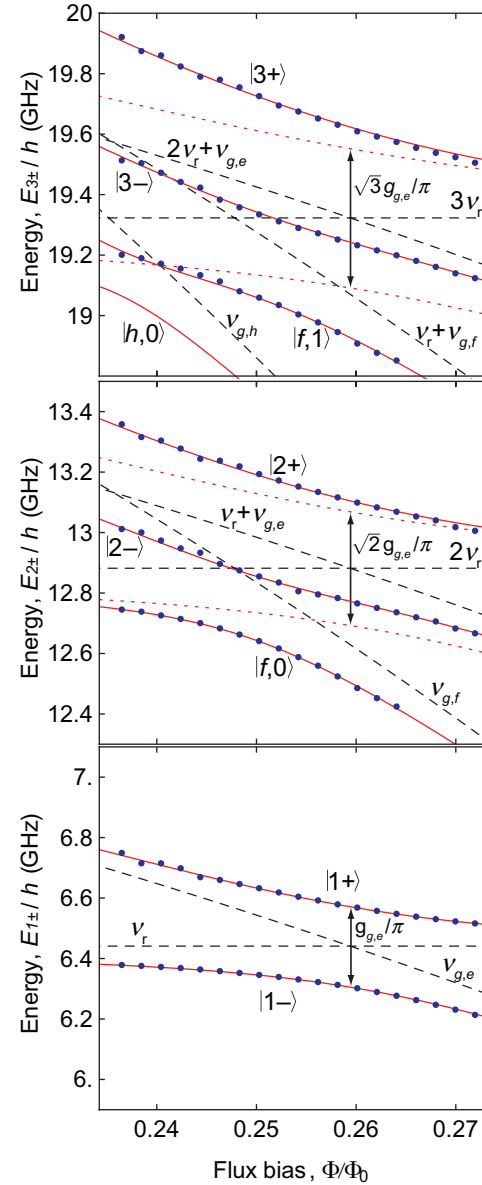


**Figure 5.** Measured energy level diagram of the three-photon/artificial atom system. Measured dressed state energies (blue dots) reconstructed from extracted transition frequencies from data in figure 4 compared to calculated uncoupled cavity and qubit levels (dashed black lines), calculated dressed state energies in the qubit two-level approximation (dotted red lines) and the corresponding calculation including four qubit levels (solid red lines).

in figure 5 that the negative anharmonicity of the transmon qubit, together with the strong dipole coupling, causes large frequency shifts of the antisymmetric dressed levels  $|2-\rangle$  and  $|3-\rangle$  as they are closer in frequency to the qubit levels  $|f, 0\rangle$ ,  $|f, 1\rangle$  and  $|h, 0\rangle$ . This leads to a small reduction of the  $\sqrt{n}$  nonlinearity, which is in agreement with the numerical results.

## 5. Vacuum Rabi mode splitting with two pump and one probe tone

In order to probe the excitation spectrum of the two- and three-photon doublet states, we can also follow the pump and probe spectroscopy scheme similar to the one

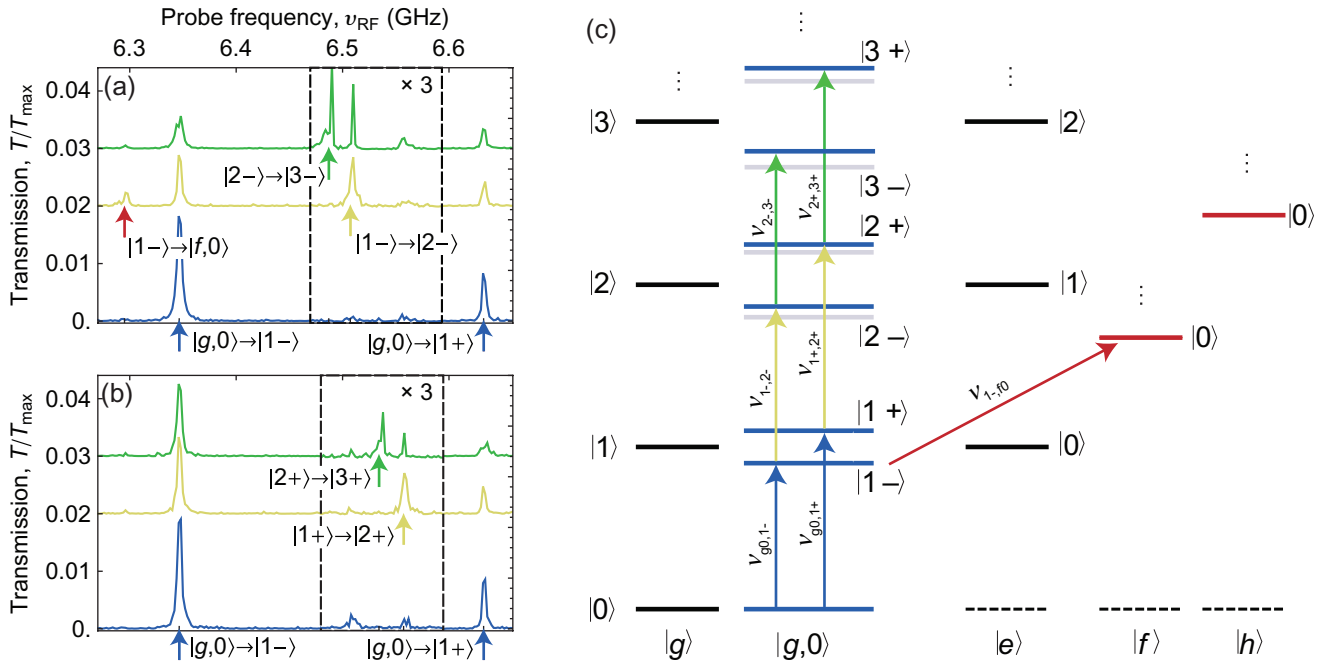


**Figure 6.** Vacuum Rabi mode splitting with one probe tone and zero, one or two coherent pump tones at flux  $\Phi/\Phi_0 \approx 0.25$  close to degeneracy. (a) Measured resonator transmission spectra  $T/T_{\max}$  without a pump tone (blue), with one pump tone  $\nu_{g0,1-}$  (yellow) and with two pump tones  $\nu_{g0,1-}$  and  $\nu_{1-,2-}$  (green) applied. The spectra are offset by 0, 0.02 and 0.03  $T/T_{\max}$  and the boxed area is scaled in amplitude by a factor of 3 for better visibility. Vertical arrows indicate numerically calculated transition frequencies. (b) Similar measurement of resonator transmission  $T$  for the case of no (blue),  $|1+\rangle$  (yellow) and both  $|1+\rangle$  and  $|2+\rangle$  symmetric dressed states pumped coherently. (c) Energy level spectrum (similar to figure 2) with relevant transitions indicated by arrows.

presented in [10, 12], where one of the first doublet states  $|1\pm\rangle$  is coherently pumped and the transition to the states  $|2\pm\rangle$  is probed. This technique avoids large intra-cavity photon numbers, which are needed in high-drive and elevated temperature experiments. In analogy to the previous section, we wait for the system to equilibrate with the cold environment to prepare the ground state  $|g, 0\rangle$ . The qubit is then tuned close to degeneracy where  $\Phi/\Phi_0 \approx 0.25$ . We weakly probe the resonator transmission spectrum as shown in figure 6 (blue lines). In a second step we apply a pump tone at frequency  $\nu_{g0,1-}$  ( $\nu_{g0,1+}$ ) occupying the dressed state  $|1-\rangle$  ( $|1+\rangle$ ) and probe the system again, see figures 6(a) and (b) (yellow line). Clearly, the transitions  $|1\pm\rangle \rightarrow |2\pm\rangle$  become visible at the calculated eigenenergy, which is indicated with red vertical arrows in figures 6(a)–(c). We also note that the state  $|f, 0\rangle$  is populated by the probe tone via the transition  $|1-\rangle \rightarrow |f, 0\rangle$ , see figures 6(a) and (c). In a last step we apply two pump tones at frequencies  $\nu_{g0,1-}$  and  $\nu_{1-,2-}$ , see figure 6(a) (green line), or at frequencies  $\nu_{g0,1+}$  and  $\nu_{1+,2+}$ , see figure 6(b) (green line), respectively. The three-photon one-qubit dressed state transitions  $|2\pm\rangle \rightarrow |3\pm\rangle$  become visible in the spectrum, see green vertical arrows. At the same time, transitions from the ground state are found to saturate considerably when the pump tones are turned on; compare the amplitudes of the spectral lines at the frequency indicated by the left (right) blue arrow in figures 6(a) and (b). This is expected since the occupation probability of the ground state is reduced and the transition starts to become saturated when the pump tones are turned on.

Again, the observed transition frequencies are in good agreement with the calculated dressed state transition energies indicated by vertical arrows in figures 6(a) and (b). Similar to the experiment described in the last section, additional spectral lines with low intensity, see figures 6(a) and (b) (blue lines), occur because of a small probability of occupation of the first doublet due to the residual thermal field. In comparison to the data shown in figure 4, no transition  $|f, 0\rangle \rightarrow |f, 1\rangle$  is observed because the level  $|f, 0\rangle$  is neither thermally nor coherently populated here.

## 6. Summary

We extended our previous work [12] by introducing thermal fields to populate the dressed eigenstates in a resonant cavity QED system. In addition to the one- and two-photon/atom superposition states, we report a measurement of the three-photon doublet using both thermal and coherent fields. The results are in good agreement with a generalized multilevel-atom Jaynes–Cummings Hamiltonian without any fit parameters. Related results have been reported in an atomic system [11] and in circuit QED [13]. Similar effects may be interesting to approach also in semiconducting cavity QED systems. It has been shown that cavity QED with superconducting circuits can be a sensitive probe for thermal fields. A more detailed quantitative analysis of the thermally excited vacuum Rabi spectra could be of interest in the context of environmentally induced dissipation and decoherence, thermal field sensing and the cross-over from the quantum to the classical regime of cavity QED.

## Acknowledgments

This work was supported by EuroSQIP, SNF Grant No. 200021-111899 and ETHZ. AB was supported by NSERC, CIFAR and the Alfred P Sloan Foundation.

## References

- [1] Raimond J M, Brune M and Haroche S 2001 Manipulating quantum entanglement with atoms and photons in a cavity *Rev. Mod. Phys.* **73** 565–82
- [2] Haroche S and Raimond J-M 2007 *Exploring the Quantum: Atoms, Cavities and Photons* (Oxford: Oxford University Press)
- [3] Walther H, Varcoe B T H, Englert B-G and Becker T 2006 Cavity quantum electrodynamics *Rep. Prog. Phys.* **69** 1325–82
- [4] Ye J, Kimble H J and Katori H 2008 Quantum state engineering and precision metrology using state-insensitive light traps *Science* **320** 1734–8
- [5] Jaynes E T and Cummings F W 1963 Comparison of quantum and semiclassical radiation theories with application to the beam maser *Proc. IEEE* **51** 89–109
- [6] Rempe G, Walther H and Klein N 1987 Observation of quantum collapse and revival in a one-atom maser *Phys. Rev. Lett.* **58** 353–6
- [7] Brune M, Schmidt-Kaler F, Maali A, Dreyer J, Hagley E, Raimond J M and Haroche S 1996 Quantum Rabi oscillation: a direct test of field quantization in a cavity *Phys. Rev. Lett.* **76** 1800–3
- [8] Varcoe B T H, Brattke S, Weidinger M and Walther H 2000 Preparing pure photon number states of the radiation field *Nature* **403** 743–6
- [9] Bertet P, Osnaghi S, Milman P, Auffeves A, Maioli P, Brune M, Raimond J M and Haroche S 2002 Generating and probing a two-photon Fock state with a single atom in a cavity *Phys. Rev. Lett.* **88** 143601
- [10] Thompson R J, Turchette Q A, Carnal O and Kimble H J 1998 Nonlinear spectroscopy in the strong-coupling regime of cavity QED *Phys. Rev. A* **57** 3084
- [11] Schuster I, Kubanek A, Fuhrmanek A, Puppe T, Pinkse P W H, Murr K and Rempe G 2008 Nonlinear spectroscopy of photons bound to one atom *Nat. Phys.* **4** 382–5
- [12] Fink J M, Goppl M, Baur M, Bianchetti R, Leek P J, Blais A and Wallraff A 2008 Climbing the Jaynes–Cummings ladder and observing its  $\sqrt{n}$  nonlinearity in a cavity QED system *Nature* **454** 315–8
- [13] Bishop L S, Chow J M, Koch J, Houck A A, Devoret M H, Thuneberg E, Girvin S M and Schoelkopf R J 2009 Nonlinear response of the vacuum Rabi resonance *Nat. Phys.* **5** 105–9
- [14] Schuster D I *et al* 2007 Resolving photon number states in a superconducting circuit *Nature* **445** 515–8
- [15] Johansson J, Saito S, Meno T, Nakano H, Ueda M, Semba K and Takayanagi H 2006 Vacuum Rabi oscillations in a macroscopic superconducting qubit LC oscillator system *Phys. Rev. Lett.* **96** 127006
- [16] Hofheinz M, Weig E M, Ansmann M, Bialczak R C, Lucero E, Neeley M, O’Connell A D, Wang H, Martinis J M and Cleland A N 2008 Generation of Fock states in a superconducting quantum circuit *Nature* **454** 310–4
- [17] Hofheinz M *et al* 2009 Synthesizing arbitrary quantum states in a superconducting resonator *Nature* **459** 546–9
- [18] Gleyzes S, Kuhr S, Guerlin C, Bernu J, Deleglise S, Hoff U B, Brune M, Raimond J-M and Haroche S 2007 Quantum jumps of light recording the birth and death of a photon in a cavity *Nature* **446** 297–300
- [19] Guerlin C, Bernu J, Deleglise S, Sayrin C, Gleyzes S, Kuhr S, Brune M, Raimond J-M and Haroche S 2007 Progressive field-state collapse and quantum non-demolition photon counting *Nature* **448** 889–93
- [20] Deleglise S, Dotsenko I, Sayrin C, Bernu J, Brune M, Raimond J-M and Haroche S 2008 Reconstruction of non-classical cavity field states with snapshots of their decoherence *Nature* **455** 510–4
- [21] Carmichael H J, Kochan P and Sanders B C 1996 Photon correlation spectroscopy *Phys. Rev. Lett.* **77** 631–4
- [22] Blais A, Huang R-S, Wallraff A, Girvin S M and Schoelkopf R J 2004 Cavity quantum electrodynamics for superconducting electrical circuits: an architecture for quantum computation *Phys. Rev. A* **69** 062320
- [23] Wallraff A, Schuster D I, Blais A, Frunzio L, Huang R S, Majer J, Kumar S, Girvin S M and Schoelkopf R J 2004 Strong coupling of a single photon to a superconducting qubit using circuit quantum electrodynamics *Nature* **431** 162–7
- [24] Schoelkopf R J and Girvin S M 2008 Wiring up quantum systems *Nature* **451** 664
- [25] A斯塔夫耶夫 O, Inomata K, Niskanen A O, Yamamoto T, Pashkin Yu A, Nakamura Y and Tsai J S 2007 Single artificial-atom lasing *Nature* **449** 588–90
- [26] Houck A A *et al* 2007 Generating single microwave photons in a circuit *Nature* **449** 328
- [27] Fragner A, Goppl M, Fink J M, Baur M, Bianchetti R, Leek P J, Blais A and Wallraff A 2008 Resolving vacuum fluctuations in an electrical circuit by measuring the Lamb shift *Science* **322** 1357–60
- [28] Deppe F *et al* 2008 Two-photon probe of the Jaynes–Cummings model and controlled symmetry breaking in circuit QED *Nat. Phys.* **4** 686–91
- [29] Baur M, Filipp S, Bianchetti R, Fink J M, Goppl M, Steffen L, Leek P J, Blais A and Wallraff A 2009 Measurement of Autler–Townes and Mollow transitions in a strongly driven superconducting qubit *Phys. Rev. Lett.* **102** 243602–4
- [30] Fink J M, Bianchetti R, Baur M, Goppl M, Steffen L, Filipp S, Leek P J, Blais A and Wallraff A 2009 Dressed collective qubit states and the Tavis–Cummings model in circuit QED *Phys. Rev. Lett.* **103** 083601–4
- [31] Majer J *et al* 2007 Coupling superconducting qubits via a cavity bus *Nature* **449** 443–7
- [32] Sillanpää M A, Park J I and Simmonds R W 2007 Coherent quantum state storage and transfer between two phase qubits via a resonant cavity *Nature* **449** 438–42
- [33] DiCarlo L *et al* 2009 Demonstration of two-qubit algorithms with a superconducting quantum processor *Nature* **460** 240–4
- [34] Koch J, Yu T M, Gambetta J, Houck A A, Schuster D I, Majer J, Blais A, Devoret M H, Girvin S M and Schoelkopf R J 2007 Charge-insensitive qubit design derived from the Cooper pair box *Phys. Rev. A* **76** 042319
- [35] Schreier J A *et al* 2008 Suppressing charge noise decoherence in superconducting charge qubits *Phys. Rev. B* **77** 180502
- [36] Bouchiat V, Vion D, Joyez P, Esteve D and Devoret M H 1998 Quantum coherence with a single Cooper pair *Phys. Scr.* **T76** 165–70
- [37] Goppl M, Fragner A, Baur M, Bianchetti R, Filipp S, Fink J M, Leek P J, Puebla G, Steffen L and Wallraff A 2008 Coplanar waveguide resonators for circuit quantum electrodynamics *J. Appl. Phys.* **104** 113904
- [38] Agarwal G S 1984 Vacuum-field Rabi splittings in microwave absorption by Rydberg atoms in a cavity *Phys. Rev. Lett.* **53** 1732–4
- [39] Sanchez-Mondragon J J, Narozhny N B and Eberly J H 1983 Theory of spontaneous-emission line shape in an ideal cavity *Phys. Rev. Lett.* **51** 550–3
- [40] Thompson R J, Rempe G and Kimble H J 1992 Observation of normal-mode splitting for an atom in an optical cavity *Phys. Rev. Lett.* **68** 1132–5

- [41] Boca A, Miller R, Birnbaum K M, Boozer A D, McKeever J and Kimble H J 2004 Observation of the vacuum Rabi spectrum for one trapped atom *Phys. Rev. Lett.* **93** 233603
- [42] Reithmaier J P, Sek G, Löffler A, Hofmann C, Kuhn S, Reitzenstein S, Keldysh L V, Kulakovskii V D, Reinecke T L and Forchel A 2004 Strong coupling in a single quantum dot–semiconductor microcavity system *Nature* **432** 197–200
- [43] Yoshie T, Scherer A, Hendrickson J, Khitrova G, Gibbs H M, Rupper G, Ell C, Shchekin O B and Deppe D G 2004 Vacuum Rabi splitting with a single quantum dot in a photonic crystal nanocavity *Nature* **432** 200–3
- [44] Zhu Y, Gauthier D J, Morin S E, Wu Q, Carmichael H J and Mossberg T W 1990 Vacuum Rabi splitting as a feature of linear-dispersion theory: analysis and experimental observations *Phys. Rev. Lett.* **64** 2499–502